Spin configurations of individual magnetic nanoflowers

Author: Inés Batalla Ferrer-Vidal
Facultat de Física, Universitat de Barcelona, Diagonal 645, 08028 Barcelona, Spain.

Advisor: Arantxa Fraile Rodríguez

Abstract: This work has consisted on processing and analysing synchrotron-based magnetic Transmission X-ray Microscopy images to obtain the internal magnetic spin texture in individual nanoflowers (NF) of about 200 nm in average size. By extracting 2D maps of the internal configuration of the magnetic moments of the cores within each NF for several tens of NF, it has been possible to visualise these different internal spin textures, all of them having in common a total magnetization close to zero. Those have been compared with previous studies, and are in agreement with prior OOMMF simulations. Due to the great variety of these configurations, a categorisation of NF subfamilies has been developed. An analysis of how the individual configurations are affected by the distance between NF has also been studied.

I. INTRODUCTION

There has been recent interest in the study of multi-core nanoparticles, for so-called nanoflowers, that are iron-oxide densely packed aggregates of cores arranged as nanoflower-like (NF) structures. This type of multi-core nanoparticles has been studied for environmental remediation as non-adsorbents or catalysts for the removal of pollutants [1].

One of the properties of NF is that despite the large size of these aggregates, and of their high saturation magnetization values, they exhibit almost zero remanent magnetization and almost negligible coercitivities [1]. The magnetic hysteresis resembles that of superparamagnetic particles, but, as the initial susceptibility is very large, the aggregates can be fully saturated under a moderate magnetic field. Previous studies propose that this behavior may be related to the existence of some kind of exchange coupling among the cores, leading to a superferromagnetic state of the whole aggregate, i.e., the magnetic correlation extends beyond the crystal grains [2]. Precisely for this reason, this magnetic correlation among the cores it is believed to be the one that gives the almost zero remanent state [3]. Simulations by OOMMF suggest that this is caused by the arrangement of the core moments in a configuration as an internal magnetization tunnel in order to minimize self-magnetic energy [4].

There be may several factors that affect the demagnetized state of the NF, such as the size distributions of the agregates, the different interactions between cores that may give rise to magnetic superstructures within a single NF, or possible supramagnetic correlations between several NF that are very close to each other [2]. The study of the specific characteristics and properties within each individual NF is therefore essential to gain both a deeper fundamental understanding as well as a control over the functionality of NF arrangements e.g., in magnetic platforms for applications such as for biomedicine and for water remediation purposes [1].

II. SAMPLE DESCRIPTION AND EXPERIMENTAL TECHNIQUE

The NF sample studied in this work, 200 nm of average size and so-called NF200, was prepared by wet chemistry routes in the group of Prof. M. Puerto Morales (ICMM-CSIC). Thereafter it was dispersed in organic solvents and deposited onto C-coated TEM grid membranes, at the chemistry lab of the Magnetic Nanomaterials Group at the UB, as thoroughly described in [1]. The table shown in Fig. 1 contains the main structural and magnetic parameters measured.

In this work, we analyzed magnetic Transmission X-ray Microscopy (M-TXM) data collected at the Mistral beamline of the ALBA light source [5] by members of the Magnetic Nanomaterials Group at the UB. The goals were first, to gain insight into the complex internal spin texture of selected NF by means of 3D magnetic tomographic characterization of the distribution of magnetic moments of the cores of individual NF. Second, to investigate if dipolar interactions may modify the intra- and inter-NF magnetic structure.

The first step was to obtain the spectra of local isotropic X-ray absorption spectra (XAS) of each NF. The TXM is a powerful and widely used tool when it comes to imaging of magnetic nanoparticles because it offers sufficient spatial resolution of a few 10nm [5]. The TXM can operate in XAS mode, scanning the same sample at different energy points across one component element's X-ray absorption edge. The reason why local XAS (not shown) were analyzed was because that way the energy that gives the largest magnetic contrast could be determined. It also confirmed the presence of the maghemite phase exact phase ($\gamma - Fe_2O_3$) across the whole volume of the NF.

Imaging of the local spin texture through the whole NF volume was carried out by using X-ray Magnetic Circular Dichroism (XMCD) as the magnetic contrast mechanism [6]. All measurements were performed at room temperature in a remanent state after ex-situ initial magnetic saturation with a near-saturating out-of-plane external

field of about 0.3 T.

XMCD reflects the projection of the local magnetization M on the photon propagation vector σ. The combination of the TXM with XMCD (also called M-TXM) provides a spatially resolved probe of the spin texture inside individual NF and of the ferromagnetic order between different NF in the ensembles. The dichroic signal is evaluated as the difference between the absorption cross-sections for right and left circularly polarized X-ray under an external magnetic field applied along the X-ray propagation vector [6]. In our case, the XMCD images were recorded by collecting right-(σ^+) and left-(σ^-) with circular polarization images at 711.2 eV, which was the energy giving the largest XMCD contrast. This measurement protocol was repeated for a series of polar rotation angles θ. Fig. 2(a) sketches the geometry used to collect the magnetic TXM images, together with the definition of the rotation angle θ.

(a)

$D_{TEM} \pm \sigma$ NF (nm)	$D_{TEM} \pm \sigma$ Cores (nm)	H_c (Oe)
186 ± 28	20 ± 4	30.8 ± 0.6

M_s (emu/g Fe_2O_3)	M_r (emu/g Fe_2O_3)
77 ± 5	5.3 ± 0.5

(b)

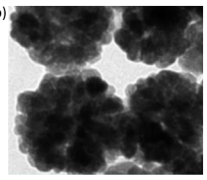

FIG. 1: (a) Table of the main structural and magnetic parameters for sample NF200 [1]. (b) High-resolution TEM (HRTEM) image of a sample of individual NF of 200 nm avarage size [1].

It should be emphasized that in general, little magnetic work has been done with this technique and the few works that exist have focused on either the characterisation of domain walls in thin films [7] and/or magnetization distribution in nanotubes [8]. In this work, we push even further this characterization to the limit since the NF is a purely 3D object and with the smallest dimensions that to our knowledge have been explored so far.

III. IMAGE PROCESSING

The whole process of image analysis has been carried out using the ImageJ software, an open-source digital image processing program [9]. In this work, a sequence of 5 XMCD images was used, corresponding to θ angles -7.5º, -5º, 0º, 5º and 7.5º. The following step was to align these 5 images extracted from XAS signal. There were organized in image stacks, a collection of images of the same region taken at these different polar angles. The alignment was done in ImageJ through a series of steps based on drift correction of an image sequence using PSI PEEM Macros (based on local FFT correlation), a measure of similarity of two series as a function of the displacement of one relative to the other. Once aligned, the ImageJ program calculated the shifts with respect to the 0º polar angle image. This way, these values could be saved and subsequently used to align the sequence of the 5 XMCD signal images.

The next thing to do was to choose the particles to analyse, but, as they were very close to each other, it was difficult to distinguish their perimeter in the XMCD stack. To tackle this problem, an ImageJ's overlay tool (acting like a mask) was used. By overlaying the XAS signal stack and the XMCD signal stack, another stack was obtained in which the perimeter of each particle was visually well distinguish. Subsequently, the particles were selected and each one of them was cut into square images of the particle size. The values for position and size were saved.

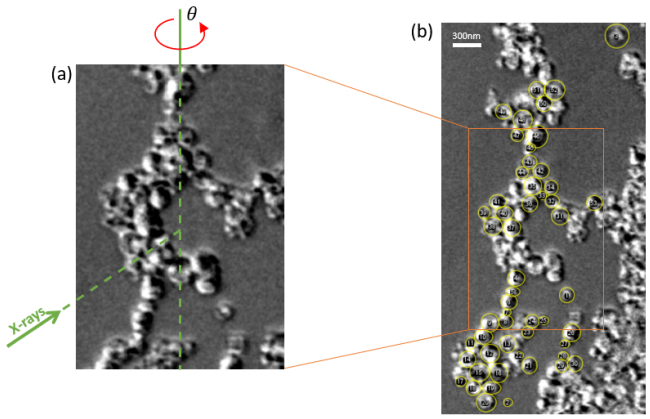

FIG. 2: (a) Sketch of incident X-ray beam/sample geometry at the MISTRAL microscope indicating the polar rotation angle θ. (b) XMCD image at $\theta = 0^{\text{o}}$, highlighting in yellow the 53 particles analized.

The extensive work of analysis and the difficulty of the method must be highlighted. Reaching this analysis protocol was the result of numerous attempts where the most relevant parameters were successively optimised. The analysis protocol described in the following represents the approach leading to the best, most consisting results. Grey scale in the XMCD images in Fig. 2 indicates magnetic contrast given by the projection of the magnetic moment along the X-ray beam direction. Thereby, bright/dark contrast corresponds to local magnetic moment parallel/antiparallel to the X-ray beam. Through a previous validation test consisting in verifying that the evolution of the magnetic moments at different θ angles followed a cosine-like behavior (see Eq. 1), it was determined that the best magnetic contrast is obtained when the signal given by the XMCD is subtracted from its background noise. For this, another ImageJ tool called "Subtract Background" was employed.

Once this procedure was done, all the particles analysed were selected in the XMCD signal stack without their background noise. In total the study was done with a statistics of 53 particles (shown in Fig. 2). Then, each particle was cut out as a square section, using ImageJ's ROI manager (Region of Interest) tool. With this tool,

the contrast level was measured from the mean grey value inside square boxes of 2x2 pixels.

In order to visualise the orientation of the magnetic moments at each ROI measured by ImageJ, the data measured by ImageJ's XMCD contrast measurement tool, has been passed through a python program developed within a previous TFG [10]. Basically, what this python program does is to calculate the conversion of our grey scale to a scale between 0^{o} and 180^{o}, i.e., each grey value implying a spin orientation. And this calculation is possible because it is known that the signal measured from the XMCD is directly proportional to the cosine of the incident X-ray angle with respect to the magnetization vector, like this:

$$\text{XMCD} \propto \cos(\vec{M}, \vec{k}) = \cos(\theta) \tag{1}$$

where $\vec{M}$ is the local magnetic moment, $\vec{k}$ the polarization vector. The diference between these two angles is θ (and it is precisely this angle θ what the python program represents over the image of a NF).

The idea of this program is therefore to produce an internal 2D map of the magnetic moments of the cores inside the individual NF. To do this, the maximum contrast value that ImageJ averaged was determined, and this value was 65535, the "brightest" white in Fig. 3(a). This corresponds to the case where the k-vector of the circular X-rays is parallel to the spin of the core, and therefore corresponds to $\theta = 0^{\text{o}}$. For this case, the program represents a blue arrow pointing to the right, at exactly 0^{o} angle to the horizontal. In contrast, for the minimum contrast value, i.e. the darkest black in Fig. 3(a), the avaraged value was 0. This corresponds to the case where k-vector is antiparallel to the spin of the core, $\theta = 180^{\text{o}}$. Therefore, in this case the program represents a red arrow pointing to the left, with an angle of 180^{o} with respect to the blue arrow pointing to the right. With these initial conditions it is possible to make this conversion from any greyscale contrast value to the corresponding angle. Note that, as $\cos(\theta) = -\cos(\theta)$, it is not possible to distinguish whether these magnetic moments are oriented in the upper or lower semicircle, therefore, it is considered for this analysis that all moments lie (and are represented) in the upper semicircle between 0^{o} and 180^{o}.

It should also be mentioned that the program considers that both the X-ray beamline and the magnetic moments are oriented out of the plane. Therefore, when the θ angles are below and above 90^{o}, the spins are pointing outwards and inwards the plane, respectively.

On the other hand, when representing the arrows, this program evaluates teh magnitude of the normalized local magnetic moment, associated to each core in the NF (1 pixel is about 7.7nm). Therefore, the higher that value, the longer the length of the arrows in Fig. 3(a). For ease of visualisation, these arrows have been represented following a color scale in Fig. 3(a).

Fig. 3(a) shows an example of this 2D map of the magnetic moments of each core for one representative NF, particularly this NF has a total magnetization of -0.0056 (in scale of -1 to 1), i.e., very close to zero, corresponding to a demagnetized state. All these 2D maps obtained for the 53 NF have been compared to simulations from [4], such as the one shown in Fig. 3(b), with approximately realistic material parameters (for a NF of size 100 nm and for the case of Hz = 0, i.e., in the absence of applied field). This simulation looks like an inner tube configuration of magnetization (the arrow in the z-direction is out-of-plane, and this is normalised between +1 and -1). In the simulation image (Fig. 3(b)), red is the white in our grayscale and blue is the black.

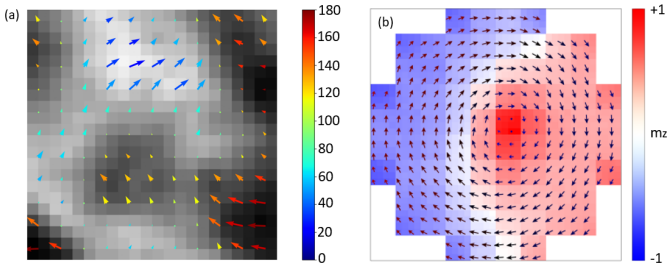

FIG. 3: (a) XMCD images with $\theta = 0^{\text{o}}$ of a selected individual NF showing the distribution of spins. The color bar on the right side indicates the θ angle between the k-vector and the spins, from 0^{o} to 180^{o}. Each pixel corresponds to 7.7 nm. (b) Simulation of the magnetization field in the z = 0 plane for zero applied field $H_z = 0$ kOe. The cell colour represents the sign of the m_z component. Taken from [4]

IV. ANALYSIS OF SPIN CONFIGURATIONS

The main objective of this work was the processing and analysis of XMCD images to obtain the spin texture within individual NF with enough data statistics. In this work, a subset of 53 NF, from a total of 500 NF, has been analyzed from which the following average total magnetization inside the NF (in a scale of -1 to 1) have been obtained: for θ = -7.5º is 0.02; for θ = -5º, -0.0057; for $\theta = 0^{\text{o}}$ 0.015; for $\theta = 5^{\text{o}}$, 0.034, and for θ = 7.5º is 0.019. Therefore, as shown in Fig. 4, we can conclude that a nearly demagnetised state is generally found, in agreement with prior simulations [4] and macroscopic magnetic parameters in Fig. 1(a).

Another factor to consider is that the avarage size of the aggregate for the sample we analysed was 186 ± 28 nm, from prior Transmission Electron Microscopy (TEM) data (Fig. 1(a)). We can make a rough estimate of the size of the 53 NF analyzed from the pixel size in the TXM experiments. From this, the average NF size in our subset of 53 NF is about 139 nm in diameter. The smallest has a diameter of 77 nm and the largest has a diameter of 215.6 nm. One of the reasons why the size determination of these particles differs from the average

NF size from the TEM data may be because the lateral spatial resolution of TXM in these experiments (1px = 7.7 nm) is 10 times worse than that of the one provided by TEM (sub-nm). Therefore, when we compare with TEM measurements they have a standard deviation of about 28 nm.

In order to see if there was any relationship between the total magnetization and the diameter of the NF and whether it is more or less demagnetised according to its size, a graphical representation was made (Fig. 4).

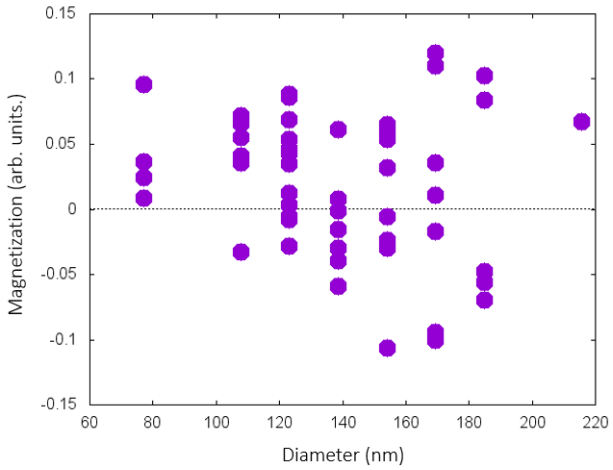

FIG. 4: Distribution of the total magnetization of NF as a function of diameter. The error bars fall within the width of the data point.

As can be seen from Fig. 4 there appears to be no apparent correlation between the size and the total magnetization of the NF. It does not seem that a larger or smaller particle prefers more or less magnetization and, instead, a total magnetization very close to zero is found regardless of the NF size.

V. TYPES OF SPIN TEXTURES

A closer look to the orientation of the local magnetic moments inside 53 different NF seem to indicate the existence of different types of spin textures within individual NF. For example, comparing the type of configuration of the simulation in Fig. 3(b) with the 2D maps obtained from the analysed particles, it has been possible to come to the conclusion that approximately 47% fall into this type of "category" of magnetization closure, similar to the simulation shown in Fig. 3(b). An illustrative example of this is the NF shown in Fig. 3(a).

Out of the total of 53 particles analysed, by the type of configuration of the magnetic moments of their cores, it has been determined that there are 3 types of categories, of "families" of NF. Apart from the category of the internal magnetization tube, hereafter called type A, there are also 22% of NF that have two relatively large black and white regions of somewhat homogeneous magnetization, resembling magnetic domains, hereafter called, type B. The remaining 31% of NF fall into an intermediate category of black, grey and white regions of comparable sizes, hereafter called type C. Illustrative examples of each case are shown in Fig. 5.

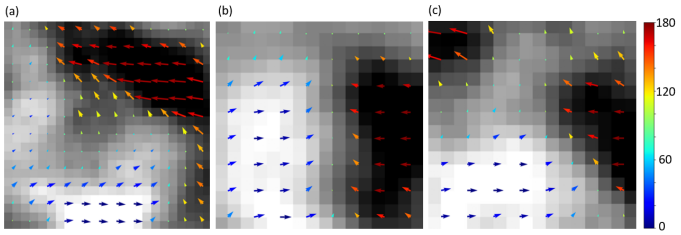

FIG. 5: Illustrative examples of Magnetic TXM images at $\theta = 0^{o}$ representative of each type of spin texture category. (a) Spin configuration "A" resembling that of the simulation shown in Fig. 3(b). (b), (c) Spin configurations "B" and "C", as described in the text. The colour bar scale is similar to that of Fig. 3(a).

After analysing and categorising these NF subfamilies according to their individual magnetization configuration, the question arose as to whether there could be any relationship between these subfamilies according to their size. A slight tendency towards more homogeneous textures (such as type B) is observed in NF with smaller sizes. In contrast, a tendency for more inhomogeneous, twisted spin textures with higher vorticity (such as type A) tends to be found in larger NF sizes. This is consistent with what is known from theory that the smaller a particle is, the more it tends to enter the superparamagnetism regime, i.e., the more difficult it is to form domains, as it tries to reduce the energy cost associated with the exchange.

VI. SPATIAL CORRELATIONS BETWEEN NF

A remarkable feature of the analysed NF is that they were apparently very close to each other, thus raising the question whether there could be some kind of spatial magnetic correlation between them. In particular, if the type of demagnetisation state of individual NF could affect that of their neighbour. To address this issue, we studied a few clusters of NF and with ImageJ we calculated the distance that separated them. Within our data statistics, it was found that NF separated by less than 3 pixels (23.1 nm) seemed to influence the demagnetisation state of the nearby NF. Above that distance, each demagnetisation state seem to be independent of the NF in question. Fig. 6 shows this effect for the case of two clusters of 3 NF (Fig. 6(a)) and 2 NF (Fig. 6(b)), respectively, separated by 1 pixel (7.7 nm) between them. Pink contours are shown as a guide to the eye to indicate how their local magnetic moments are "connected".

On the one hand, this is not surprising because typi-

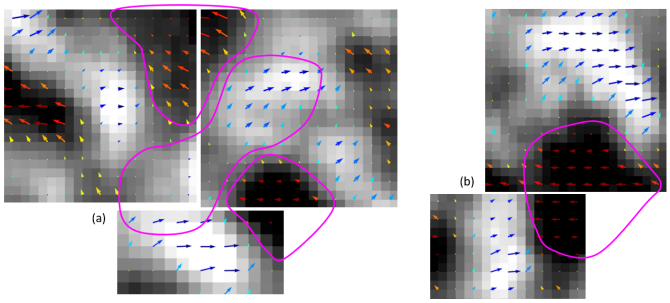

FIG. 6: (a) 3 NFs close together (b) 2 NFs close together. Both NF clusters show how the internal spin texture affects each other. Pink contours are a guide to the eye to highlight this effect in a qualitative way.

cally all analysed particles fall into a state of individual magnetization each of them very close to zero. Magnetically speaking this implies that the stray field of the NF is very small, very close to zero, and it is near to another NF which is also practically demagnetised. Therefore, as the two respective stray fields are very small, their dipolar interaction is small [11]. Consequently, only for a very small distance, magnetic dipolar correlations seem to set in. Nevertheless, care must be taken while analysing the interparticle correlations results, considering that the statistics of analysed clusters is very low and the TXM technique is not accurate enough for measuring distances, as explained earlier.

VII. CONCLUSIONS

In this work, the image processing and analysis of a short tomographic series of magnetic Transmission X-ray Microscopy images has been performed with the goal to determine the distribution of magnetic moments of the cores of individual magnetic nanoflowers. It has been shown that the NF are practically demagnetised at zero applied field in agreement with prior magnetic simulations. Tens of magnetic NF have been analyzed. Different spin arrangements inside the NF have been observed, ranging from spin textures with high vorticity in almost half of the cases to configurations with two seemingly large domains with opposing magnetization or other more complex configurations. The second goal was to investigate how the individual configurations are affected by dipolar interactions between NF. It has been found that below a certain distance spatial magnetic correlations are visible.

This type of measurements are very innovative and the analysis is very challenging, as the characterization done in this TFG is of a purely 3D object with the smallest dimensions that, to our knowledge, have so far been explored. Nevertheless, in order to better quantify the information we would need more complete tomograms with a small angle step and ideally tomograms at different azimuthal angles, but this requires additional measurements not available in the context of this TFG.

Acknowledgments

I would like to deeply thank my advisor Arantxa Fraile Rodríguez for these months that she has been guiding me with this final degree project. I also want to thank Leila Belmonte, who helped me to better understand her python code. And finally, I want to thank my family and my closest friends, not only for this project but also for all these years of career, for always supporting me and believing in me.

[1] Mariona Escoda. Tuning the performance of magnetic, semiconductor, and multifunctional hybrid nanostructures. PhD thesis, Universitat de Barcelona, 2022.
[2] Bender, P. et al, J.Phys. Chem. C, 122, 3068 (2018).
[3] C. Blanco-Andujar. High performance multi-core iron oxide nanoparticles for magnetic hyperthermia: microwave synthesis, and the role of core-to-core interactions. Nanoscale, 7:1768–1775, 2015.
[4] Iker García. Magnetic properties of iron oxide nanoflowers. TFG, Universitat de Barcelona. 2022.
[5] Pereiro E, Nicolás J, Ferrer S, Howells MR. A soft X-ray beamline for transmission X-ray microscopy at ALBA. J Synchrotron Radiat. 2009 Jul;16(Pt 4).
[6] XMCD microscopy with synchronized soft X-ray and laser pulses at PETRA III for time-resolved studies. P Wessels (2013).
[7] Hermosa-Muñoz, J., Hierro-Rodríguez, A., Sorrentino, A. et al. 3D magnetic configuration of ferrimagnetic multilayers with competing interactions visualized by soft X-ray vector tomography. Commun Phys 5, 26 (2022).
[8] C.Donnelly et al, Nature Nanotechnology 17, 136 (2022).
[9] Schindelin, J., Arganda-Carreras, I., Frise, E., Kaynig, V., Longair, M., Pietzsch, T., ... Cardona, A. (2012). Fiji: an open-source platform for biological-image analysis. Nature Methods, 9(7), 676–682 (2019).
[10] Leila Belmonte. Direct observation of spin textures in magnetic nanoflowers. TFG, Universitat de Barcelona. 2022.
[11] P. Bender, D. Honecker and L. Fernández Barquín. Supraferromagnetic correlations in clusters of magnetic nanoflowers. Appl. Phys. Lett. 115, 132406 (2019).